Nuclear Instruments and Methods in Physics Research A 386 (1997) 23-31

NUCLEAR INSTRUMENTS & METHODS IN PHYSICS RESEARCH Section A

ELSEVIER

The OPAL Phase III microvertex detector

Sijbrand de Jong *

Indiana University, Physics Department, Swain Hall West 117, Bloomington, IN 47405, USA

For the OPAL microvertex group

Abstract

A description of the OPAL Phase III microvertex detector is given. Special emphasis is put on problems that have been encountered in the installation and operation of the different phases of the OPAL microvertex detector leading to the present Phase III detector and their cures. A short description of the new OPAL radiation monitoring and beam dump system is also given.

1. Introduction

A fully detailed description of the OPAL microvertex detector can be found in Refs. [1-3]. This presentation is aimed to be complementary to the information described in the papers above and to a presentation by Ö. Runolfsson at the Hiroshima conference [4], that discusses the problems and solutions in the manufacturing of the OPAL microvertex (and other) detectors. Several features are exposed here, that are normally not discussed in the standard detector NIM papers, but are relevant for the successful operation of this particular microvertex detector. Short descriptions of the main parts of the OPAL detector and of the OPAL microvertex detector in particular are embedded to make this presentation more or less self-contained.

2. Short description of the OPAL Phase III detector

2.1. The OPAL detector

OPAL [5] is a general purpose detector operated at the e^+e^- LEP collider at CERN in Geneva, Switzerland. The detector consists of a central tracking system in a solenoidal magnetic field of 0.435 T, surrounded by electromagnetic calorimeters (including pre-samplers), hadron calorimeters and muon chambers. In the forward direction, close to the beam pipe, on each side luminosity monitors are mounted. The central tracking system consists of three sets of wire chambers in a 4 bar gas tank. The large-volume jet chamber (CJ) has 24 azimuthal sectors of 159 wires each and goes out to a radius of nearly 2 m. Inside the jet chamber is a high-precision vertex chamber (CV) with 36 azimuthal sectors of 12 axial and 6 stereo wires. On the outside of the jet chamber are chambers with their wires arranged perpendicular to the beam direction to measure the z coordinate (CZ). In the annular space between the pressure chamber holding the wire chambers and the beam pipe is the silicon microvertex detector (see Fig. 1.)

Without silicon microvertex detector the impact parameter resolutions are $\sigma(d_0) = 35\ \mu$m for high-momentum isolated tracks that have all possible jet and vertex chamber hits and $\sigma(z_0) = 1.1$ mm for high-momentum isolated tracks that have all possible jet and z chamber hits. Impact parameter resolutions for OPAL including the silicon microvertex detector are discussed in one of the following sections.

2.2. The OPAL microvertex detector history

In 1991 the first phase of the silicon microvertex detector was installed [1]. In the Phase I detector there were two barrels of 11 and 14 ladders, respectively, where the ladders did not overlap in the azimuthal coordinate. Single-sided FoxFET silicon wafers [6] were used. Hence there was only one coordinate available. These silicon detector wafers are about 60×33 mm^2 with a thickness of about 300 μm. The p+ strips are spaced by 25 μm and every other strip is read out by an AC coupled metal strip, giving a readout pitch of 50 μm. These wafers will subsequently be called ϕ wafers.

In 1993 the Phase II silicon microvertex detector was installed [2]. The Phase II detector had the same concept as Phase I, but utilised single-sided wafers with strips in the orthogonal direction to the Phase I wafers (subsequently called z wafers) which were glued back-to-back onto the Phase I ϕ wafers. The z wafers have p+ strips implanted

* Permanent address: PPE division, CERN, CH-1211 Geneva 23, Switzerland. E-mail: sijbrand.de.jong@cern.ch.

PII S0168-9002(96)001091-1

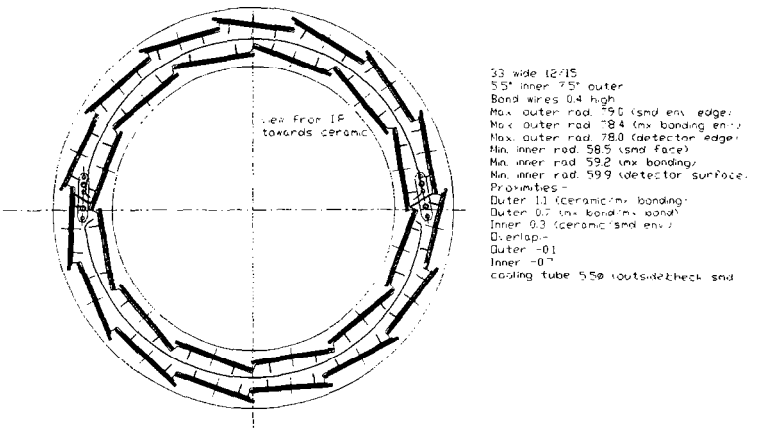

Fig. 1. Cut in the transverse direction of the OPAL silicon microvertex detector. The constraining space is formed by the wall of the pressure vessel on the outside and the beam pipe on the inside.

every 25 μm and every fourth strip is read out by an AC coupled metal strip, giving a readout pitch of 100 μm. Other than the strip orientation the z wafers are very similar in design to the ϕ wafers. The thickness of both the ϕ and z wafers in Phase II was limited to 250 μm to reduce multiple scattering. The Phase II mechanical and electrical structure is rather similar to what is used in the Phase III detector and will be described below.

In 1995 OPAL was equipped with a silicon microvertex detector that was in between the Phase II and Phase III situation. The mechanics was already changed such that 12 inner barrel ladders and 15 outer barrel ladders were used to close the gaps in the azimuthal coordinate. In the Phase III detector two types of ladders are used: long ladders that contain three wafers lined up one after the other and short ladders that contain two of these wafers. However, not enough short ladders could be manufactured in time, so that only the long ladders, which got carried over from Phase II, were used. The detector was centred in OPAL on the long ladders and the short ladders that were present in the outer barrel were ignored for physics analyses. The technical experience gained by installing the Phase III mechanical structure and part of the short ladders showed very valuable for the installation of the full Phase III in 1996. In addition the running of a significant subset of the short ladders gave full confidence of the operational stability of these objects.

In 1996 the full Phase III detector was installed closing both the azimuthal coordinate gap, as well as making the detector longer by 5/3 in the direction along the beam [3].

2.3. The OPAL Phase III microvertex detector

The Phase III OPAL microvertex detector is built up of ladders that contain the silicon detector wafers and the signal multiplexing electronics. Two types of ladders are used: long ladders that contain three wafers lined up one after the other and short ladders that contain two of these wafers. An exploded schematic view of a long ladder is shown in Fig. 2. The silicon wafers are of the FoxFET type and were manufactured by Micron Semiconductors Ltd. Their dimensions are 60×33 mm^2. Two types of silicon wafers are used: ϕ wafers that have strips in the long direction of the wafer, and z wafers that have strips in the short direction of the wafer. On both wafer types p+ strips are implanted every 25 μm. On the ϕ wafers every other strip is read out by an AC coupled metal strip (readout pitch of 50 μm) and on the z wafers every fourth strip is read out this way (readout pitch of 100 μm). The ϕ and z wafers, each about 250 μm thick, are glued back-to-back to form an object that detects two orthogonal coordinates for passing tracks. Wafers on a ladder are daisy chained by bonding their ϕ readout strips between the wafers. For z wafers the readout strips are bonded to a glass backing plate called z-print with metal strips printed on it. The metal print on the glass backing plate is arranged such that the z strips of the two or three wafers on a ladder are daisy chained and are fanned out to the short side at the

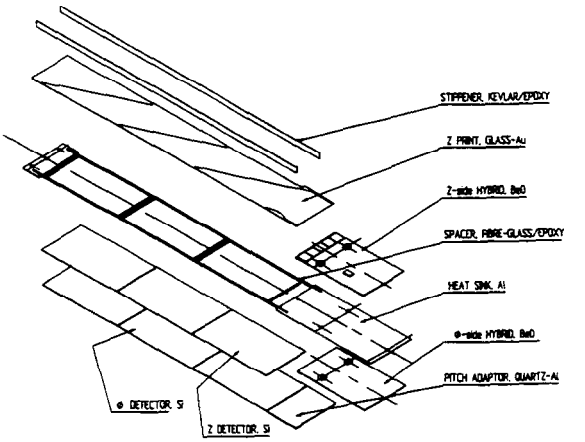

Fig. 2. Exploded view of an OPAL long ladder.

end of the backing plate. On both sides the pitch of the detectors is adapted to the pitch of the readout chips. On the ϕ side this is done by a separate pitch adapter of metal print on quartz or glass and on the z side the pitch adapter is integrated in the glass backing plate print. The wafers, glass backing plate and pitch adapter are all glued to a thin fibre/epoxy frame. Stiffener ribs of kevlar/epoxy are glued to the back of the z-print to give rigidity to the ladder structure.

The front end electronics at the end of the ladders consists of two BeO ceramic plates that are glued back-to-back on a thin Al plate. The Al plate is used to attach the electronics to the glass backing plate and ϕ pitch adapter. The Al plate is also used to screw the ladders to support rings to form the detector ensemble and serves as the heat sink for the heat generated by the electronics on the BeO plates. The electronics on the BeO plates (one side for ϕ and on the back for z) consists of five MX7 microplex chips, each reading 128 channels, a sequencer chip to generate the control signals for the MX7 chips and some linear networks used for filtering power lines. The MX7 chips on the long ladders are of the original type, whereas for the short ladders a radiation hard version of the MX7 chip was used.

The ladders are mounted on metal and carbon fibre support rings in a two-barrel arrangement. The ladders are tilted with respect to a tangent geometry to have a mechanical overlap. There is no overlap in the sensitive area of the detectors, but the dead space between the sensitive areas of adjacent ladders is negligible. Long and short ladders are matched up in the length direction to effectively form ladders of 5 wafers of which 3 are read out on one side and 2 on the opposite side. Mechanical rigidity of the overall assembly is given by two Be half shells that are between the two barrels. The long and short ladders are only fixed firmly to Al support rings at the electronics end. The end of the ladders away from the electronics are near the centre of the OPAL detector and are held in place by supports of foam between thin carbon fibre sheets holding two hollow Be pins. These supports are glued on the Be half shells. Small pieces of carbon fibre with holes that fit around the Be pins of the support are glued onto the end of the ladders. The Al support ring on each side that has the electronics of the ladders attached to it has a stainless steel tube soldered onto it to provide cooling by flowing water through it. The side where all the long ladders are attached is the left-hand side, and the side of the short ladders is the right-hand side.

The front end electronics on the ladders connects with small connectors to inter connect ring cards (ICR cards) of which there are seven on either side of the assembly. The ICR cards incorporate one more stage of multiplexing, sequencing the signals of two ladders in series. The signals are then sent to the counting room using balanced amplifiers. The ICR cards also contain the receivers for the control signals and a sequencer chip. The mechanical structure of the ICR cards is further used to support radiation monitors, on which more details will be given in a later section.

The ICR cards have all the cables soldered onto them and these cables run for approximately 2 m along the beam pipe and then pass another 3 m along the luminosity detectors and the mini-beta magnet in the LEP ring. They then connect up to a patch tower that rearranges the cable groups and thicker cables are run from there for 25 m to the counting room. The patch tower is located between the hadron calorimeter and the muon chamber in the forward direction. In the counting room the cables connect to a power supply system, a control and monitoring system and the DAQ system.

The power supplies are controlled by the control and monitoring system that also controls and monitors the cooling system and monitors various other parameters of the detector, notably about 60 temperatures.

The DAQ system consists of a VME crate that contains three processors, one to connect to the OPAL event builder and trigger that also serves for general tasks as interactive login and data monitoring and two that are dedicated to read out the left and right-hand side of the detector, respectively. The readout system for both sides is the same and consists of a fastbus crate that contains an interface to the VME processor, a master sequencer module (MSEQ) and 14 Sirocco modules. The master sequencer module arranges all the timing aspects of the sample and hold of the MX7 and the readout synchronisation between front end electronics and Sirocco modules. The Sirocco modules receive the multiplexed analog signal from the MX chips and digitise these signals and store them in front end buffers. The digital information in the front end buffers is then being processed by digital signal processors (DSPs) that keep record of pedestal and noise values of each channel and sparsify the data to only keep hit clusters. The data for hit clusters is transferred into a crate end buffer from where it is read through the fastbus-VME interface by the dedicated processor in the VME crate. The DSPs also histogram various quantities to monitor data quality and DSP performance.

3. Installation procedure

The microvertex detector was only introduced as a concept to OPAL at the time the experiment was already completed for initial data taking. It was only by merit of shrinking the beam pipe radius from 8 cm to 5 cm allowed by LEP that the microvertex detector could be added without drastic, and practically impossible, changes to the OPAL detector that was already in place. Therefore, only the annular space between the pressure pipe, that forms the wall of the pressure vessel for the wire chambers, and also served as beam pipe for the early running of the experiment, and the new Be beam pipe is available to install a microvertex detector. This puts rather severe limitations to the geometry to fit this space, but no less important also to the installation strategy. The microvertex detector has to be moved down the pressure pipe for more than 2 m with the beam pipe in place. It is impossible to insert the beam pipe with the microvertex detector in place. The beam pipe layout was fixed by the

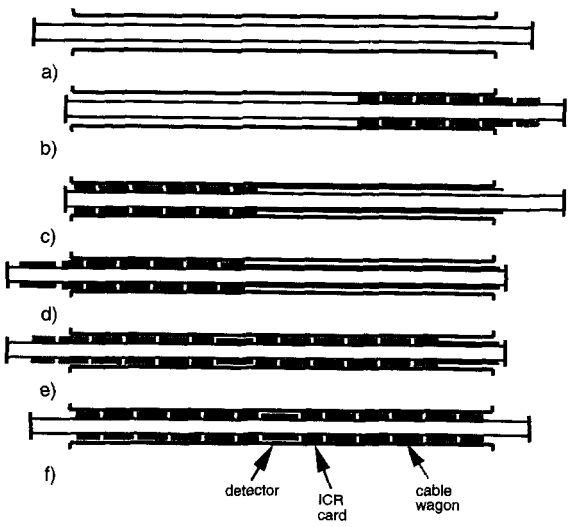

Fig. 3. Installation procedure of the OPAL microvertex detector. In (a) the geometry of the pressure pipe (part of the wire chamber pressure vessel) and the beam pipe are shown schematically. In (b) the ICR cards are introduced from the right-hand side followed by cable support wagons. In (c) the right-hand side ICR cards and cable wagons are pushed all the way to the left-hand side, the second part of this pushing operation is performed by rods and temporary cables supports. In (d) the detector is attached to the right-hand side ICR cards. Then in (e) the left-hand side ICR cards are attached and the detector is moved to the centre of OPAL, while putting in cable support wagons for the left-hand side. Finally in (f) the beam pipe is centred in OPAL again.

geometry of the luminosity detectors in the forward direction and the position of the flanges is such that only a limited amount of the beam pipe can be exposed outside of the flanges of the pressure pipe. In fact for the installation of the Phase III microvertex detector the available length between the beam pipe and pressure pipe flanges is not enough with the beam pipe in its final, more or less symmetric, position. Therefore, the beam pipe is moved inside the pressure pipe during the installation of the Phase III microvertex detector. Another complication in the installation procedure is the fact that cables to the microvertex detector have to come out at both ends of the pressure pipe.

All these complications result in an installation procedure that is sketched in Fig. 3. In Fig. 3a the geometry of the pressure pipe (part of the wire chamber pressure vessel) and the beam pipe are shown schematically. In Fig. 3b the ICR cards are introduced from the right-hand side followed by cable support wagons. To facilitate this operation the beam pipe is moved towards the right-hand side, although this is not strictly needed. The ICR cards as well as the cable support wagons are mounted as two half cylinders around the beam pipe. The cable support wagons are introduced as five cylinders that are attached one to the other. The cable support wagons are supported by the pressure pipe, because the beam pipe is supposed not to be touched by anything. The cables and cooling tubes are arranged around the cable support wagons such that the weight of the ensemble rests on the plastic tubes of the cooling tubes and a plastic tube that guides small cables that control a beam pipe support mechanism close to the ICR cards. In Fig. 3c the right-hand side ICR cards and cable wagons are pushed all the way to the left-hand side, the second part of this pushing operation is performed by rods and temporary cables supports. At this stage of the operation there have been problems with the friction of the cables onto the pressure pipe when they were not properly supported. This was cured by doing the temporary cable support more carefully. Next in Fig. 3d the detector is attached to the right-hand side ICR cards. This is done after the functionality of the right-hand side ICR cards is tested before anything is connected to them. After the detector is connected to the right-hand side ICR cards the short ladder side is tested in situ. After this verification the left-hand side ICR cards are attached. At this point the entire detector is tested. The position of the detector at that time allows access to the left-hand side, but not to the right-hand side any more as that has already disappeared inside the pressure pipe. Then in Fig. 3e the detector is moved to the centre of OPAL, while putting in cable support wagons for the left-hand side. At the final position the detector is tested again before finishing the cable fan out etc. Finally in Fig. 3f the beam pipe is centred in OPAL again. After the beam pipe has been put in its final position it is supported from the pressure pipe near the end flanges and near the middle close to the right-hand side ICR cards. The microvertex detector itself is also fixed in position by a clamping ring that is operated by steel wires passed out with the cables in a separate plastic tube. During all the above operations stress is put on the fragile cables that come out from the detector. These cables are custom made to fit the space available, while arranging them homogeneously around the beam pipe to least influence the luminosity measurement.

Problems have frequently been encountered with a type of cable that combines four groups of group-shielded twisted pair cables for detector signals with five groups of unshielded twisted pair cables for temperature monitoring in one sleeve. The temperature monitoring cables can wrinkle up and break when the loops are stretched again due to freedom remaining even after the sleeve has been tightly stretched. Several repairs in situ have been made to recover all the temperature readings.

The position of the microvertex detector in OPAL is measured by the distance between a marker on a wire and the end flange of the pressure pipe. The distance between the marker on the wire and the point where the wire is attached to the detector has also been measured, as well as the point the wire is attached to the detector with respect to other reference points on the detector. This allows one to put the detector in position to about one millimeter in the direction along the beam. There is no mechanism to control the rotation around the beam axis of the detector very well. Rotations with respect to the nominal position of the detector between 0 and 4 degrees have been observed after installation over the different years. The shift along the beam and

the rotation angle around the beam of the entire structure are easily measured from the data using only few events and pose no problem.

4. Operational experience

Concerning the operations of the OPAL microvertex detector three specific items will be discussed. Apart from an overheating accident that will be discussed as one of them the OPAL microvertex detector has been running very successfully. However, it needs be noted that since its first installation as Phase I in 1991, it has been extracted from OPAL and reinserted every year. Three times this has been due to planned upgrades, the other two times a number of failures developed that made it worth to extract the detector, repair it and reinstall it again.

4.1. Leakage current rises

From the start of the operation of the Phase II detector it was noticed that leakage currents were unstable when the detector bias was switched on for a long time. Notably increases of leakage current in coincidence with radiation incidents were observed. For some of the ladders these leakage current increases were monotonic and a plateau was never reached before action was taken to prevent further rise. The maximum leakage current that was observed for a particular ladder was 30 μA, whereas in normal operation the maximum leakage current is about 1 μA per ladder. This problem was cured in the experimental environment by introducing a standby voltage for the detector backplane. This voltage is matched to the voltage on the signal side of the wafers, so that there is no potential across the wafers. Between physics runs, when LEP is filling etc., these standby voltages are activated. Since this procedure is in operation small leakage current increases are observed during physics runs but this mostly recovers between the runs when the detector is put to standby. However, a very slow trend to increase leakage current is still seen on the time scale of a year for some ladders.

The leakage current problem has been investigated in detail using several methods. A significant number of ladders, but not all, that have the radiation induced leakage current rise, also have a similar problem in a high relative humidity environment ($>$ 70% RH.) In different test beams the radiation induced leakage current was tried to be provoked under controlled conditions. In the CERN LPI beam that delivers relativistic electrons in bursts of 10^8–10^{10} an increase of leakage current has been observed once on one ladder, but could never be reproduced again. Since the problem could not be reproduced, the LPI irradiation was given up after testing a single ladder and some single wafers. Two ladders have been irradiated in an X-ray source with photons of similar energy to the LEP synchrotron radiation. Dose rates of 10 rad/minute and integrated doses of several hundred rads were given to the ladders. One time a leakage current was observed that ran away, but again the effect could later not be reproduced, neither on the same ladder, nor on the other ladder.

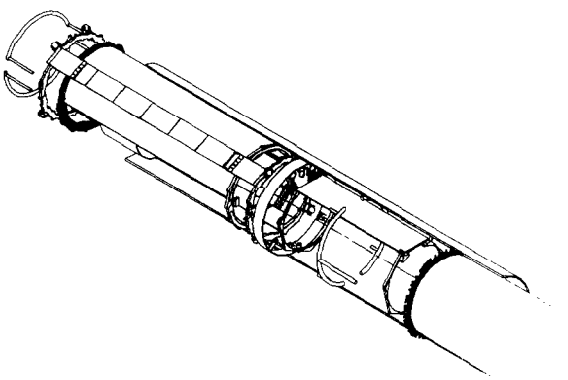

Fig. 4. The OPAL Phase III microvertex detector schematic view. Only one long and short ladder pair is shown and one ICR card.

Being unable to reproduce the radiation-induced leakage currents in a controlled environment and having observed some correlation between radiation sensitivity and humidity sensitivity, the leakage current rise due to humidity was subsequently used to test wafers in the construction period for the Phase III detector. In the course of the project, when the failure rate in the humidity test became very high, wafers that failed the test were baked in a vacuum oven after which many of them passed the same leakage current test, which overcame the yield problem. It should be pointed out that in the OPAL environment the detector is kept under a dry nitrogen atmosphere and relative humidity is never larger than a few percent at the microvertex detector. During the construction period detector wafers and ladders are as much as possible stored in boxes that are flushed with dry nitrogen.

4.2. Overheating incident

Due to a bad combination of several failures the OPAL microvertex detector ran in 1994 for a short while without cooling water flow. As a result the temperature of the detector rose to over 100°C. This lead to most of the ladders failing subsequently. After the detector was taken out, many of the failures were found to be just bias bond wires that were broken and most of the ladders could be repaired fairly easily. Some ladders needed more extensive repairs of the bond wires, but in the end all ladders involved in the incident were repaired and regained their original efficiency.

One of the causes for the overheating incident was a failing interlock. The reason for the failure was that it was in bypass state, which was probably true for some time but never noticed by the shift crews or detector experts. This observation lead to implementing a new and more rigorous interlock system.

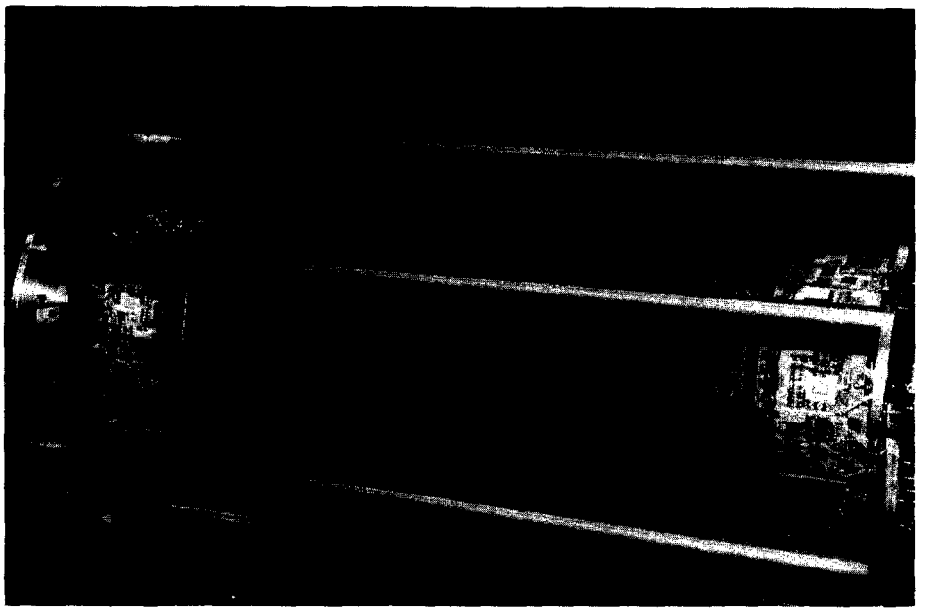

Fig. 5. The OPAL Phase III microvertex detector prior to installation.

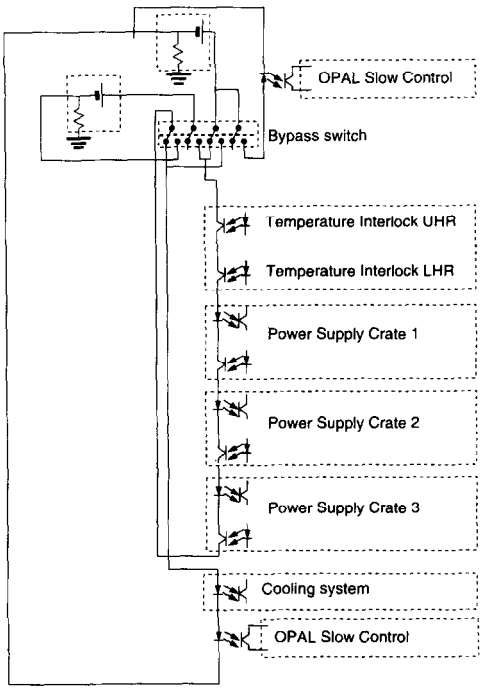

Fig. 6. Schematic of the OPAL microvertex interlock system.

This new system interlocks the power system, the cooling system and the temperature monitoring system by means of a current loop. This is drawn schematically in Fig. 6. If any of these three systems stop functioning, or are in an anomalous state a current loop is broken and both the power and the cooling system switch off by interrupting their power. A bypass switch is still needed during installation when various parts of the system are tested independently, but overriding the interlock system with the bypass switch is reported as error condition to the OPAL shift crew automatically and the shift crew is instructed to bring this to the attention to the microvertex detector experts immediately and subsequently at regular time intervals. This avoids bypasses to exist unintentionally or for more time than necessary. The experience with the new interlock system is very good, based on its functioning during installation, when bypasses were used, and based on its reaction to failing equipment and general power failures.

4.3. *Automation of monitoring*

A problem with an experiment that is already running for more than six years is that hardware experts tend to leave for new and more challenging projects and the detector has to be maintained by a small group of people. This problem has been attacked by automating the system as much as possible.

All the monitoring functions can be performed from any workstation in the world. By logging in to the online system all hardware parameters can be displayed on a screen and DAQ histograms can be viewed to judge data quality. A limited standard set of histograms is also periodically inspected by the OPAL shift crews. In addition all hardware functions, like starting and stopping the power and cooling system, changing parameters in these systems and even resetting the monitor CPU can be performed remotely. The only thing that is left manual is the reset of a hard tempera-

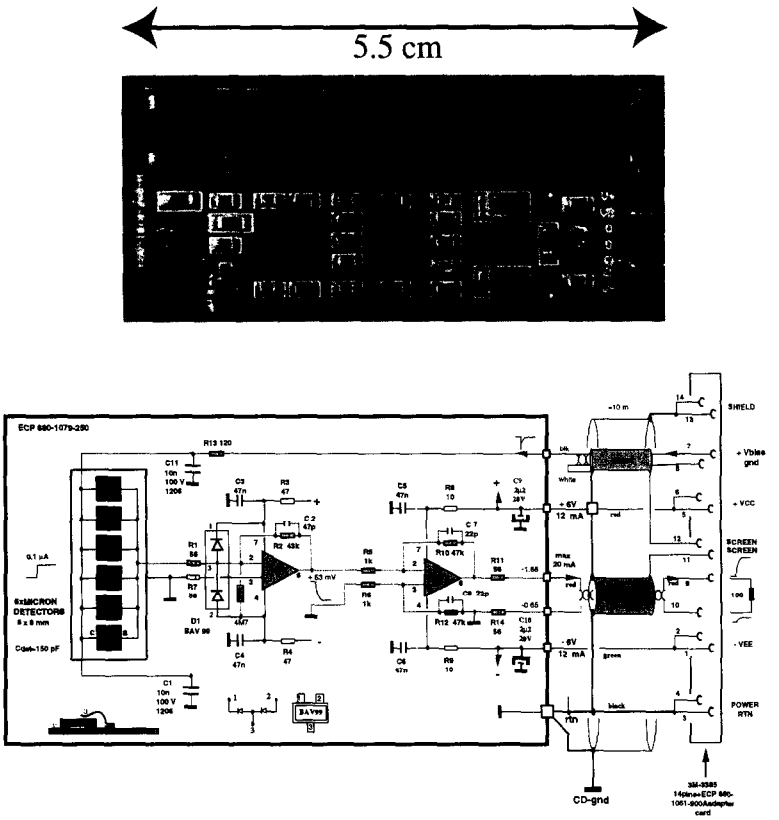

Fig. 7. Radiation monitor front end cards in real life (top picture) and in schematics (bottom picture).

ture interlock exception. This condition is judged sufficiently severe that it merits a hardware expert to be forced to go to the counting room. So far this situation has never occurred.

Part of the operations has also been automated. The ramping up and down of the detector, which is a sequence of actions on the cooling and powering system where feedback is needed from the temperature to judge when to ramp the power is dealt with by a program. The interference of the operator is limited to giving commands to bring the detector up or down. The cooling system itself is controlled by a program that changes the cooling parameters to keep a constant temperature on some specific parts of the detector. In case the monitoring software finds repeatedly anomalies that could possibly affect the safety of the detector, relevant parts of the detector are ramped down automatically and put in a safe position. Of course this generates fatal error messages and noises in the OPAL control room on which experts are notified.

5. Radiation monitoring and beam dump system

From the beginning a radiation monitoring system was installed with the microvertex detector. The original radiation monitors consist of four solar cells which are left unbiased and on which the charged generated by radiation is measured. This charge is converted in a frequency at the patch tower and transported to the control room where it is converted to a voltage that is measured by an ADC. The use of a frequency to transport the signal makes the signals slow and the rise and fall time is of the order of 1 second. The total amount of charge that was generated is conserved by the signal treatment, making this system useful to measure total radiation doses and making a history profile accurate to one second. Remarkably enough a small fraction of solar cells have a very small temperature sensitivity in their charge production. These were selected for use in the experiment after fake radiation detection due to temperature variations had caused problems and could not be easily corrected for by software (due to hysteresis in temperature versus charge creation, the absence of thermistors very close to the solar cells and limitations in the accuracy of temperature monitoring.)

After an incident in which 150 microplex channels were destroyed by a pencil-like beam it was realised that very fast detection of radiation and response to fast rising radiation by means of a beam dump is desirable. For this purpose a new set of radiation monitors was developed and installed. These new radiation monitors use 8×8 mm^2 test diodes from the detector wafers. A number of these diodes are connected in

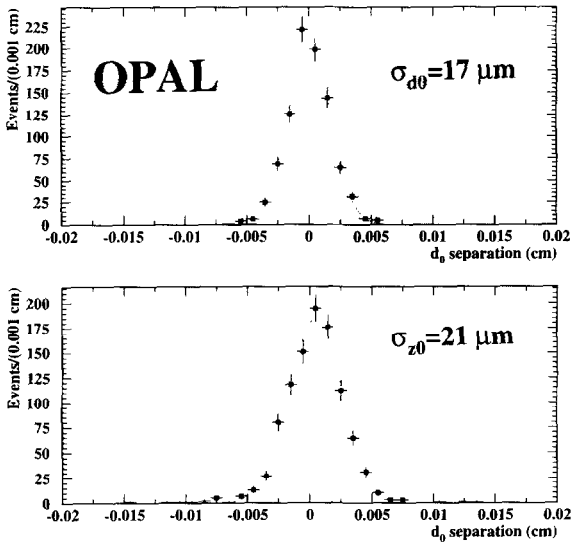

Fig. 8. Impact parameter resolution in the plane transverse to the beam (d_0) and in the direction along the beam (z_0) for $e^+e^- \rightarrow Z^0 \rightarrow \mu^+\mu^-$ events, where the μ tracks are perpendicular to the beam direction.

parallel and reversed biased. The signals from these diodes are proportional to the charge liberated in the diodes, which in turn is proportional to the radiation dose. These signals are preamplified and transported to the counting room. In the counting room the signal are split in a signal path that is shaped with a time constant of the order of 1 second for integrated dose measurements and a fast signal that is used in a beam dump circuit that responds to very high doses in very short time intervals.

After various trails in OPAL with the new radiation monitors it was realised that they observe significantly more radiation than the old solar cells. This can be explained by several facts. The solar cells have a lower intrinsic sensitivity, as they are unbiased. But even more important, the solar cells are positioned on the ICR cards facing away from the beam pipe. Therefore, certainly for small-angle tracks, they have a significant amount of material between the sensors and the beam. The new radiation monitors are mounted on the side of the ICR cards facing the beam pipe and have very similar exposure to the beam as the inner barrel ladder detector wafers. The response to off-momentum particles and particle showers is not so very different for the old and new monitors, but the response to synchrotron radiation differs by more than a factor of 10.

It was also realised that it is impossible to serve an accurate integrated dose measurement, for which sensitivities of about 50 mrad/hour are desirable, and a beam dump system for which the lowest sensitivity is 1 rad/s. Therefore, the new system was further upgraded to use in addition to the amplified signal from the front end cards, also the signal over the decoupling capacitor for the backplane bias voltage. This allows one to have a total dynamic range of about 10^8 from combining the two signal paths. The final front end card is shown in Fig. 7.

To avoid saturation problems due to high leakage currents, the silicon diodes for the radiation monitor cards were subjected to similar leakage current stability tests as the detector wafers. Only very stable diodes were retained for use in the radiation monitors.

Both the amplifier signal as well as the backplane signal of the radiation monitor front end cards are treated very similar in the counting room. The signals are terminated by 120 Ohm over a large capacitor and the signal over the termination resistor is AC coupled to a differential amplifier. The RC time of the capacitor at the input of the differential receiver amplifier is chosen such that the input signal is differentiated. The differentiated signal is then rectified. This rectified differentiated signal is still proportional to the charge created in the diodes on the front end card, although the constant of proportionality depends critical on the signal shape that results from the ensemble of amplifiers. This is not a problem as the properties of this ensemble of amplifiers is proven to be very stable and the channels are calibrated one by one using test input signals. The rectified differentiated signal is fanned out to both a shaper with an RC time of 1 second for an integrated dose measurement as well as to a beam dump module.

The beam dump module integrates the fast rectified differentiated signal, but bleeds the integrated charge at a constant, but adjustable, rate. This decay rate is currently set to 1 rad/s. This means that radiation levels under 1 rad/s will remain unnoticed by the beam dump circuit. Levels over 1 rad/s will integrate up and when the integral exceeds a certain level an alarm or dump bit will be set. Presently the alarm and dump levels are set to 0.5 and 1 rad. The beam dump circuit distills a beam dump signal from at least one channel above dump level and a settable number of channels above alarm level.

The radiation monitor and beam dump system is set up independently for both the left- and right-hand side of the detector.

The radiation monitors have proven stable in operation and need no temperature corrections. The beam dump system has been operational in a mode in which the beam dump signal is not sent to the LEP machine for a short period of time this year. Last year a prototype beam dump system similar to this years has been operated, without sending dump signals to LEP, for a period of time too. The joint experience of these two trail periods is that beam dumps that would have been triggered by this new system were always in situations in which the beam was lost in a short while anyway. However, in some cases the radiation that was received by the OPAL microvertex detector could have been significantly limited if this beam dump system would have been active.

6. Results for physics

As a highlight of the OPAL silicon microvertex performance the impact parameter resolution for $e^+e^- \rightarrow Z^0 \rightarrow \mu^+\mu^-$ is shown. The impact parameter resolution in the direction along the beam (z) has greatly improved over what has been reported in [2]. Many different improvements in alignment have contributed to this result. But the biggest improvements were due to a retuning of the tracking parameter uncertainties for the entire central tracking system as a function of track momentum and the fitting of the effective radius from the detector centre of ϕ and z wafers separately. The latter actually gives rise to relative positions of the ϕ and z wafers that are unphysical, but this might be understood in terms of alignment compensating for other inaccuracies in describing the hit positions, e.g. due to biases in clustering or readout strip pitches that are slightly different from the nominal ones.

7. Conclusions

Since 1991 OPAL has a silicon microvertex detector in operation. The microvertex detector has gone through three phases of increasing sophistication and coverage of solid angle. The presently installed Phase III microvertex detector is the final phase and will serve until the end of the LEP era (which is foreseen around the year 2000.) The OPAL physics program has greatly benefited from the presence of the microvertex detector. For the LEP2 high energy running the main function of the microvertex detector will be the recognition of Higgs particles that decay in b quarks. It is hoped that soon examples of positive identification of Higgs bosons with the help of the microvertex detector can be shown.

Acknowledgements

In addition to the acknowledging the hard work of the entire OPAL microvertex detector group, two engineers, who have carried out a large part of, respectively, the mechanical and electronical design and construction need to be mentioned specifically: Bill Glessing and Robert Hammarström.

Mario Caria and the other organisers of the VERTEX96 workshop are warmly thanked for bringing us to Sardinia and mixing stimulating presentations with other pleasures of life.

References

[1] P.P. Allport et al., Nucl. Instr. and Meth. A 324 (1993) 34.
[2] P.P. Allport et al., Nucl. Instr. and Meth. A 346 (1994) 476.
[3] P.P. Allport et al., The extended OPAL Silicon Microvertex Detector with two coordinate readout, to be submitted to Nucl. Instr. and Meth.
[4] Ö. Runolfsson, Quality Assurance and Testing before, during and after Construction of Semiconductor Tracking Detectors, CERN-PPE/95-163.
[5] OPAL Collaboration, K. Ahmet et al., Nucl. Instr. and Meth. A 305 (1991) 275.
[6] P.P. Allport et al., Nucl. Instr. and Meth. A 310 (1991) 155.
[7] O. Biebel et al., The OPAL Silicon Microvertex Detector Radiation Monitoring and Beam Dump System, to be submitted to Nucl. Instr. and Meth.